Energy

Numerical investigation of a dual cylindrical OWC hybrid system incorporated into a fixed caisson breakwater

--Manuscript Draft--

Manuscript Number:	
Article Type:	Full length article
Keywords:	wave energy; oscillating water column; wave resonance; combined system; energy conversion efficiency
Corresponding Author:	Lars Johanning
First Author:	CAN YANG
Order of Authors:	CAN YANG
	Lujun Zhao
	Chang Wan
	Hengxu Liu
	Tingting Xu
	Daqing Wu
	Hailong Chen
	Lars Johanning
Abstract:	In this paper, a hybrid breakwater-OWC system combining heaving floater Wave Energy Converters (WEC) was investigated. The traditional cylindrical-type breakwater consists of dual cylinders with an opening inlet located at the outer wavefront wall, allowing a ring-type wave chamber formed between two cylinders. The oscillating buoy OB is hinged at the front of the OWC device. Based on the Computational Fluid Dynamics (CFD) software Star CCM+, A three-dimensional numerical wave tank is developed to investigate the hydrodynamic performance of the hybrid system, and the numerical model is validated with published experimental results. The power take-off (PTO) damping performance and the hydrodynamic efficiency affected by water conditions and geometrical dimensions of the device are discussed. Results show that the after combining the floater to the breakwater-type WEC, a great improvement on frequency bandwidth was achieved and maximum wave energy conversion efficiency can approach 83.28% for this proposed hybrid system. It was found that the opening height ratio of h1/h2=0.4 has the largest conversion efficiency for the tested regime. Lower height ratio of the opening inlet of the OWC chamber should be avoid for larger water depth condition while designing such a hybrid system.
Suggested Reviewers:	Nigel Barltrop nigel.barltrop@strath.ac.uk
	Tessa Gordelier T.J.Gordelier@exeter.ac.uk
	Hongjie Wen wenhongjie@scut.edu.cn

Numerical investigation of a dual cylindrical OWC hybrid system incorporated into a fixed caisson breakwater

Can Yang[a,b], Lujun Zhao [a,b], Chang Wan[a,b], Hengxu Liu [a,b,*], Tingting Xu [a,b], Daqing Wu [a,b], Hailong Chen [a,b], Lars Johanning [a,b,c,*]

[a] Yantai Research Institute and Graduate School, Harbin Engineering University, Yantai 265500, China

[b] College of Shipbuilding Engineering, Harbin Engineering University, Harbin 150001, China

[c] College of Engineering, Mathematics and Physical Sciences, University of Exeter, Penryn Campus, Penryn, Cornwall, TR10 9FE, UK

Abstract: In this paper, a hybrid breakwater-OWC system combining heaving floater Wave Energy Converters (WEC) was investigated. The traditional cylindrical-type breakwater consists of dual cylinders with an opening inlet located at the outer wavefront wall, allowing a ring-type wave chamber formed between two cylinders. The oscillating buoy OB is hinged at the front of the OWC device. Based on the Computational Fluid Dynamics (CFD) software Star CCM+, A three-dimensional numerical wave tank is developed to investigate the hydrodynamic performance of the hybrid system, and the numerical model is validated with published experimental results. The power take-off (PTO) damping performance and the hydrodynamic efficiency affected by water conditions and geometrical dimensions of the device are discussed. Results show that the after combining the floater to the breakwater-type WEC, a great improvement on frequency bandwidth was achieved and maximum wave energy conversion efficiency can approach 83.28% for this proposed hybrid system. It was found that the opening height ratio of h_1/h_2=0.4 has the largest conversion efficiency for the tested regime. Lower height ratio of the opening inlet of the OWC chamber should be avoid for larger water depth condition while designing such a hybrid system.

Key word: wave energy; oscillating water column; wave resonance; combined system; energy conversion efficiency

1 Introduction

With the increasing concerns of the global warming and climate change, under the highly oil prices and the peak oil environment, government has shifted more support to increase renewable energy incentive policies, legislation and commercialization [1]. Thereby, an increasing number of countries starting to transfer their focus on renewable energy to achieve the sustainable development [2]. Among the various renewable energy resources, ocean energy and particularly the wave energy have gained great attention due to its potential advantages of providing huge substantial energy all over the world, which has been roughly estimated between 1 and 10 TW [3-4]. Amongst them, type of the Oscillating Water Column (OWC) and Oscillating Buoy (OB) wave energy converters (WEC) have been widely applied for wave energy utilization and studied in literature [5]. Because of the high cost of the WECs, combining them into other ocean engineering structures can greatly improve the equipment viability and saving the economic cost [6]. The idea of the integration of the breakwater and WECs was first proposed by Graw [7]. Currently, the WECs integrated into the breakwater have been initially developed and tested in sea

states [8], such as the Sakata plant (60KW) in Japan [9], the Pico plant (400KW) in Portugal [10], the Mutriku plant (296 KW) in Spain [11], the LIMPET (500 KW) in England [12], the Shanwei OWC plant (100KW) in Guangdong, China [13].

Evolving from the original concept the OWCs now being many variations, experiencing the upgrading and updating. Zheng et al. [14] developed a theoretical model based on linear potential flow theory to study the performance of a coast/breakwater-integrated OWC. The results showed that the more perpendicular the incident wave direction relative to the coast/breakwater, the more wave power that can be captured by the OWC. Shi et al. [15] carried out physical model tests on the caisson breakwater-OWC device, the experimental results showed good stability and feasibility of the device. Gonçalves et al. [16] developed a 2D CFD model based on the software FLUENT aiming to study the influence of the air compressibility effect inside the OWC chamber. Results showed that air compressibility effects can diminish the predicted OWC efficiency up to about 20% in both Wells and impulse turbines. Rodríguez et al. [17] proposed a numerical model to investigate the effects of the front wall thickness and the bottom profile of the OWC on the conversion efficiency performance. The numerical results revealed that a thinner front wall of the OWC can obtained wider efficiency band, but with less capacity to withstand the impact of storm waves.

In addition to the traditional single chamber OWC acting as breakwater, other forms of OWC model were also proposed to improve the wave energy absorption. Ning et al. [18] conducted an experimental study on a land-based dual-chamber OWC. The results were compared with a typical single-chamber OWC device, which showed an improvement in both the maximum efficiency and the effective frequency bandwidth. Then, Wang et al. [19] further studied the wave loads on the dual-chamber OWC. It was shown that the joint of device and seabed suffered the largest wave moment. Besides, other researchers investigated the stepped bottom effects of the dual-chamber OWC analytically and numerically [20-21], which indicated that under the stepped sea bottom conditions, the dual-chamber OWC have better performance in the wave power extraction compared to single-chamber OWC device within wide range of frequencies. Furthermore, as previously studied, the cylinder-type caisson breakwater is more stable especially for severe wind-wave conditions [22]. Chen et al. [23-24] proposed a novel dual cylindrical caisson breakwater double as an OWC device and investigated the wave energy conversion performance in the experiments. The experimental study demonstrated that the peak efficiency of the integrated system is inversely proportional to the incident wave height, while the resonant incident wave period corresponding to the peak efficiency is affected by the water depth.

Meanwhile, as another main type of the WECs, there are many relatively studies dealing with the Oscillating Buoy (OB) devices integrated into the breakwater. Zhao et al [25-26] studied a breakwater-type WEC composed of fixed and floating pontoons through analytical and experimental investigations, and improved conversion efficiency was found due to the integrated system. Zhang et al [27] proposed a dual-floater hybrid system combining a floating breakwater with an OB-WEC by using Star-CCM+ software. The results showed that wave resonance in the WEC-breakwater gap has a significant impact on system performance, with the hybrid system demonstrating both better wave attenuation and wave energy extraction capabilities at low wave frequencies, i.e., wider effective frequency. Zheng and Zhang [28] analytically studied a hollow cylindrical OWC with a long floating cube hinged and found that the interaction between the OWC and OB is advantageous to the wave energy extraction for certain wave conditions. Another hybrid WEC system consisting of a hollow cylindrical OWC with several OB hinged around was also analytically studied by 3D semi-analytical model [29]. The results showed that the hybrid WEC system could have a wider bandwidth frequency and higher wave energy conversion

compared with the isolated OWC and OB. Cui et al [30] also studied this proposed analytical model and found that the combined system has a positive influence on the wave energy capture.

In this paper, a hybrid WEC system composed of a hinged floating OB and a cylindrical caisson breakwater acting as an OWC device was presented. The proposed dual cylindrical OWC with two baffle walls in the hollow chamber was fixed on the seabed. To investigate both the hydrodynamic behavior and the power extraction performance of the integrated system, a three-dimensional numerical model was developed by using CFD two-phase flow method. This paper is organized as follows. Section 2 described the numerical model, including the boundary conditions and its mesh generation. The validation of the numerical model compared with the experimental results, and the flow field characteristics in and around the hybrid system were also given in this section. Section 3 presented the PTO damping effects of both the OWC and OB on the coupled system. The hydrodynamic performance of the combined system was discussed in Section 4, and Section 5 further analyzed the effects of the geometrical properties of the OWC-OB system on the wave energy conversion efficiency. Finally, the concluding remarks were given in Section 6.

2 Mathematical model

2.1 Numerical wave tank setup

The sketch of the numerical setup of a hybrid system of a fixed caisson breakwater combined with an oscillating buoy type WEC operating under wave conditions was shown in Figure.1, allowing only the heave motions of the buoy floater in normal incident waves. As shown in Figure.1, the radius of the oscillating floater is R_i, D presents the distance between the OB and the OWC's geometrical center. The radius of the outer cylinder and the inner cylinder of the OWC are R and r, respectively. For the fixed OWC device, the total water depth of the inner chamber is h, the height of the opening inlet is h_2, the distance between the upper edge of the opening inlet and the water surface is d_1, and the thickness of the front wall of the OWC device is set as 10mm. A circular nozzle is arranged on the top cover of the OWC with an opening radius of r_i, and the distance between the nozzle and the OWC cylindrical center along x-axis is of l=2/3R (see Figure.1(b)).

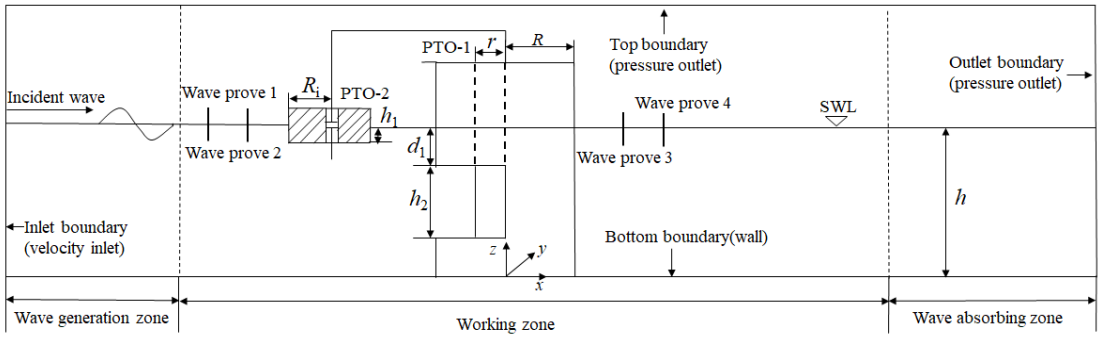

(a)

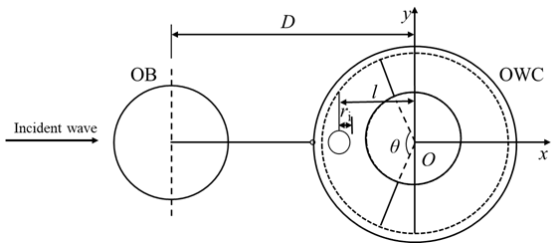

(b)

Fig.1 Definition sketch of the hybrid OWC-OB device for (a) front view; (b) vertical view

The inlet boundary condition of the numerical tank was set as the velocity inlet, the velocity of the fifth-order VOF wave was set to inlet surface velocity vector, and fluid field was set as the water and air two-phase flow. The vertical velocity(W) and the horizontal velocity (U) of the fifth order VOF wave are given by

$$U=\frac{\partial \Phi}{\partial X},\ W=\frac{\partial \Phi}{\partial Z} \tag{1}$$

where X is the horizontal co-ordinate, Z is the vertical co-ordinate in the Cartesian coordinate system, and Φ is the velocity potential given by

$$\Phi\left(X,Z,t\right)=\left(c-\bar{u}\right)X+C_0\left(\frac{g}{k^3}\right)^{1/2}\sum_{i=1}^{5}\varepsilon^i\sum_{j=1}^{i}A_{ij}\cosh jkZ\sin jk\left(X-ct\right) \tag{2}$$

$$\bar{u}\left(\frac{k}{g}\right)^{1/2}=1+\frac{1}{2}\varepsilon^2+\frac{1}{8}\varepsilon^4+\mathrm{O}\left(\varepsilon^6\right) \tag{3}$$

in which c is the wave propagation velocity, k represents the wave number, A_{ij} and C_0 are the model coefficients, g is gravitational acceleration, and $\varepsilon=kH/2$ is the nondimensional parameter compared to wave amplitude. The outlet boundary and the upper boundary were set as the pressure outlet, and the fluid static pressure was specified as the fifth-order VOF wave. A no-slip wall boundary condition was assigned to the bottom of the domain. To simulate that the WEC device operated in the exposed waters area, both sides of the calculation tank were set to symmetry boundary conditions. Furthermore, to avoid the backflow of waves at the exit of the tank, stretch grid type mesh for 0.5m long were set at the exit area.

The mesh involved in the numerical model was generated by using Star-CCM+-Meshing software. In order to save the CPU time and maximize the calculation accuracy, trimmed grid model was used to mesh the calculation area. The detailed mesh generation of the wave tank model is shown in Figure.2, a subtracted area on the Oscillating Buoy floater was introduced when it was placed in the tank, its body surface was set as the no-slip boundary conditions in the numerical model, and the overset mesh condition was set for the outer surface. The concentrated meshes were assigned to the motion zone, the overlapping mesh zone and the export zone of both the OWC and OB model. Besides, a region of three times of incidence wave height at the free surface was set with fine mesh, which was stretched from the device model to the boundaries. To ensure the energy transfer between the background grid and the overlapping grid correctly, the size of the overlapping mesh was set to be equal with that at the motion zone.

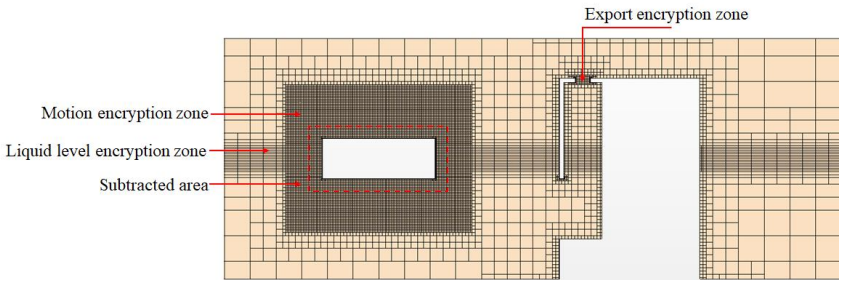

Fig.2 Mesh generation details of the wave tank model.

2.2 Validation of the CFD model

In order to validate the present CFD model, a typical cylindrical OWC structure fixed on the sea bottom was set up and simulated to reproduce Chen & Wang's [23-24] experiment results. The tank tests were performed in the basin of the State Key Laboratory of Coastal and Offshore Engineering in Dalian, China. The wave tank was 40m in long, 24m in wide, and 1m in depth. Typical cases with condition of the water depths of 0.3m and 0.4m, the incident wave heights of 0.03 and 0.06 m, and the wave periods from 0.7 to 1.1s were tested in the modelling. The dimensions of the numerical water flume, the proposed model and the environmental conditions including the water depth, the incident wave properties, the geometrical parameters of the opening inlet, the outer/inner diameters of the dual cylindrical caisson type OWC device were set the same with the physical tests. More specially, the total height of the OWC device was 0.5m, the nozzle sectional area S was 46mm×40mm, the shell thickness b was 5mm, the chamber breadth B was 0.38m, the height of the opening s was 0.15m, and the lower edge of the opening was 75mm. Further details could be found in Ref. [24].

The wave energy conversion efficiency of the typical cylindrical OWC was given and compared between the numerical and published experimental data, as is shown in Fig.3. Two water depths of d_1=0.3m and d_2=0.4m, with two different incident wave height of H=0.03m and 0.06m were chosen for validation. In the Figure, the hollow squares and circles represent the numerical results, and the solid squares and circles represent the experimental results. It can be seen that the experimental and numerical results perform a good agreement, allowing the wave period range from 0.7 to 1.1s. For d_1=0.3m, the maximum error of the wave energy conversion efficiency between the measured and calculated values were 8.79% with H=0.03m and 7.86% with H=0.06m. Whilst for d_2=0.4m, the maximum difference of the conversion efficiency is 12.08% for H=0.03m and 3.03% for H=0.06m, respectively.

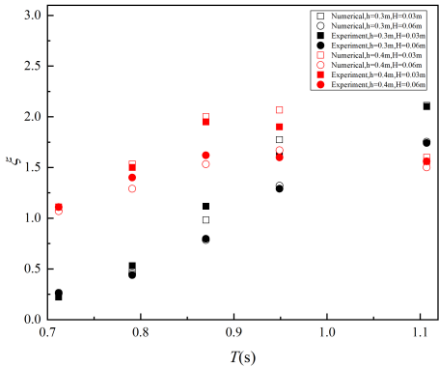

Fig.3 Comparison of the wave energy conversion efficiency of the OWC model between numerical and experimental results.

The aforementioned comparisons and validation analysis indicate that the present numerical model matches well with the experiment, and it is able to reproduce the processes of the wave-structure interactions for the proposed dual cylindrical caisson type OWC device. Thus, further study will base on this calibrated numerical model.

3 Analysis of PTO damping

3.1 PTO damping of OWC device

In this subsection, the PTO damping of the OWC device for the integrated system is studied. Falcao et.al [31] have indicated that for the power conversion of the impulse turbine the damping effect is independent of the turbine rotational speed approximately, and this speed involved in the maximum

power conversion efficiency of the OWC can be selected without affecting the hydrodynamics during first-stage energy harvesting. That is to say, the damping effects and the hydrodynamic performance of the OWC device can be evaluated separately after simulating the impulse turbine model. The PTO damping coefficient D^* can be expressed as follow [32]:

$$D^* = \frac{K}{|q_{\mathrm{AP}}|} \tag{4}$$

where K is the pressure characteristic parameter defined as

$$K = \frac{S_{\mathrm{w}}\sqrt{|p_{\mathrm{OWC}}|}}{\sqrt{\rho_{\mathrm{A}}}} \tag{5}$$

With the orifice at the outlet, the air flow rate in the nozzle and the air pressure in the chamber are conducted, respectively. The relationships between the air flow rate and air pressure for different wave conditions are shown in Fig.4. From the figure almost cubic nonlinearity relations between the air flow rate and air pressure could be observed. For water depth of h=0.3m, the total air pressure p_{OWC} and the air flow rate q_{AP} in the chamber nozzle increased with the increasing of wave height. The relative large range of the air flow rate is -0.014~0.013m^3/s, and the air pressure in the chamber of the OWC variated from -54.95Pa to 23.17Pa for the wave height of H=0.06m, which was almost three times larger than that with the case of H=0.03m for the same water depth condition. Compared to the wave height effects, the obtained data of the air pressure and the air flow rate with different water depths were drawn in Fig. 4(a) and Fig. 4(c). With the increase of the water depth, the values and the variation range of the air flow rate and the air pressure characteristics increased but not larger than that of the wave height effects.

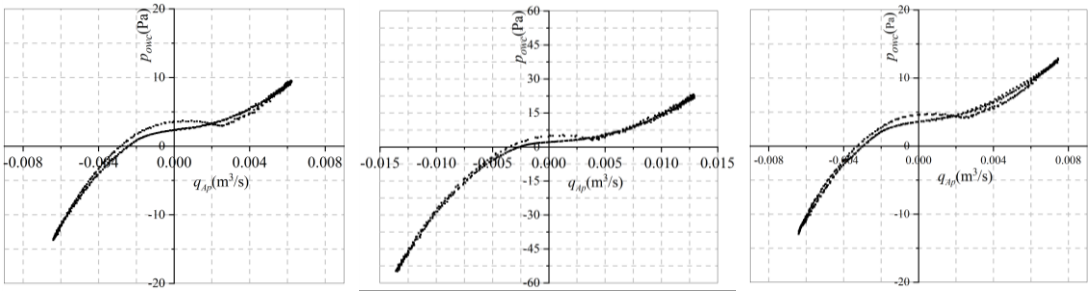

(a) (b) (c)

Fig.4 Quadratic relationships between the air flow rate (q_{AP}) and the air chamber pressure (p_{OWC}), for (a) h=0.3m, H=0.03m, T=0.95s (b) h=0.3m, H=0.06m, T=0.95s (c) h=0.4m, H=0.03m, T=0.95s.

The relationships between the feature parameters of air pressure and air flow rate are shown in Fig.5. As seen in the figure, the characteristic parameter of the air pressure increases approximately linearly with the increasing air flow rate, with the slope of the fitted curves representing the damping coefficient $D^*$of the PTO system (see Fig.5(a), 5(b) and 5(c)). The pressure characteristic parameter was averaged in the air exhaust and suction modes to evaluate the damping effects. It can be observed that there are two curves relative to the PTO damping coefficient values obtained from the simulated results in the OWC chamber, which can be considered as one is the PTO damping coefficient of the OWC itself, and the other one represents the PTO effects caused by the oscillating buoy located in front of the OWC. Hence, for the hybrid OWC-OB integrated system operating under different conditions, both the air turbine damping of the OWC and the PTO damping of the OB could be adjusted to increase the power conversion efficiency of the OWC device. In addition, the incident wave height and water depth have an

important influence on the PTO damping coefficient of the OWC device. For condition of the water depth of h=0.3m, the corresponding PTO damping coefficients (for H=0.03m) are 43.23 and 19.86, and when the wave height increase to H=0.06m, the PTO damping coefficients increased to 34.17 and 17.47, respectively. For further increasing the water depth to h=0.4m(H=0.06m), the values of the PTO damping coefficients are 49.60 and 17.32, as is shown in Fig. 5(c). It indicates that the effect of the water depth on the damping coefficients of the OWC device is larger, while the factor of the wave height impacting on that of the floater OB is more sensitive.

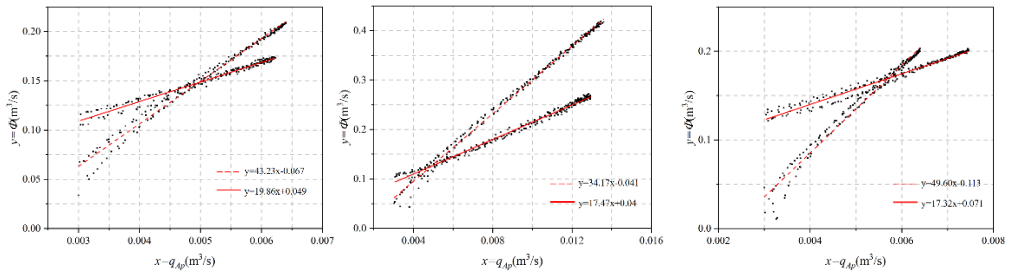

(a) (b) (c)

Fig.5 The pressure characteristic parameter K versus the air flow rate $|q_{AP}|$, for (a) h=0.3m, H=0.03m, T=0.95s (b) h=0.3m, H=0.06m, T=0.95s (c) h=0.4m, H=0.03m, T=0.95s.

3.2 PTO damping of OB device

The oscillating buoy was constrained to allow heave motion only, thus the motion equation of floater can be written as

$$m\ddot{z} + b_{\text{pto}}\dot{z} + c_{\text{pto}}z = -mg + F_{\text{w}} \tag{6}$$

where m represents the floater mass; b_{pto} and c_{pto} are the mechanical parameter of the damping and elastic stiffness caused by the PTO system, respectively; F_{w} is the total wave loads (including the buoyancy of the floater); z, $\dot{z}$ and $\ddot{z}$ are the motion response, motion velocity and the motion acceleration of the floater, respectively.

The initial frequency of the model structure was used to define the resonant frequency as the restoring loads and the inertial loads are in equilibrium [33], that is

$$\omega_{\text{n}} = \sqrt{\frac{c_{\text{pto}} + c_{\text{z}}}{m + a_{\text{z}}}} \tag{7}$$

The relationship between the optimal PTO damping coefficient b_{opt} and the wave frequency ω can be described as [34]

$$b_{\text{opt}} = \sqrt{\frac{\left(\left(m + a_{\text{z}}\right)\omega^2 - \left(c_{\text{pto}} + c_{\text{z}}\right)\right)^2}{\omega^2} + {b_{\text{z}}}^2} \tag{8}$$

in which $c_{\text{z}}=\rho g A_{\text{w}}$ is the restoring loads coefficient that caused by the contribution differences from the buoy weight and the hydrostatic term, A_{w} is the buoy wetted surface, a_{z} (added mass coefficient) and b_{z} (radiation damping coefficient) are the functions of the wave frequency, which were obtained in a 3-D numerical wave tank using potential-flow theory [34-35].

Fig.6 shows the variations of the wave energy conversion efficiency η against different PTO damping coefficients for the hybrid system with three typical wave periods, with condition of H=0.03, d=0.3m. The relative damping coefficient $b_{\text{pto}}/b_{\text{opt}}$ was used to evaluate the PTO damping effects for optimization. It can be seen that there is an apparently increase of the OB conversion efficiency η

occurred within the range of b_{pto}/b_{opt}=0.2-0.5, when the damping ratio b_{pto}/b_{opt} variated in the range of 0.5-1.25, there is little difference of the conversion efficiency between different damping ratios (see Fig.6). It can be included that for the damping coefficient b_{pto} is less than half of the optimal damping coefficient b_{opt}, the PTO damping is the key influencing factor for evaluating the wave energy conversion efficiency of the OB device. For the three incident wave periods shown in Fig.6, the maximum conversion efficiency all occurred at the case of b_{pto}/b_{opt}=1, which illustrates that potential flow theory provides an accurate method for determining the optimal damping b_{opt}. Furthermore, with the increase of the wave period, the wave energy conversion efficiency of the device decreased especially for longer waves. It indicates that the OB device has good power extraction performance for shorter waves. In the following sections, the hydrodynamic characteristics and the wave energy conversion performance of this proposed hybrid system will be analyzed in detail.

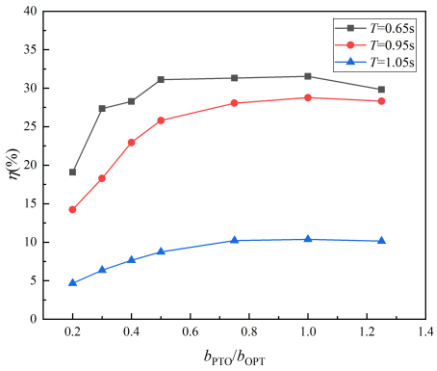

Fig.6 Power conversion efficiency η with different PTO damping coefficients

4 Hydrodynamic performance

4.1 Hydrodynamic Performance of the Combined System

To study the hydrodynamic behavior of the combined system, the transmission coefficient K_t, the reflection coefficient K_r and the dissipation coefficient K_d were involved for evaluation with different wave parameters. Two wave heights were selected as H=0.03m and 0.06m, allowing the water depth equal to 0.3m and 0.4m. The transmission coefficient K_t and the reflection coefficient K_r are defined as follows

$$K_t = H_t / H_I \tag{8}$$

$$K_r = H_r / H_I \tag{9}$$

where H_t is the transmission wave height, H_r is the reflection wave height, and H_I is the incident wave height. The transmission wave height H_t was measured at the points behind the combined system with the Two-point method, as the same the reflection wave height H_r was measured at the points in front of the system. The two points of measuring the reflection wave height were set at x_1=-1.49m and x_2= x_1-0.25L, and the measured points for transmission wave height were located at x_3=0.65m and x_4=x_3+h, respectively.

The dissipation coefficient K_d due to the energy dissipation caused by the fluid viscosity effect is defined as

$$K_d = 1 - K_t^2 - K_r^2 - \eta \tag{10}$$

where η is the wave energy conversion efficiency.

To investigate the power extraction performance of the proposed integrated system, the transmission

coefficient, reflection coefficient and the dissipation coefficient of the OWC-OB system under different incident wave heights at water depth of h=0.3m and 0.4m are shown in Fig.7 and Fig.8, respectively. For condition of water depth h is 0.3m, it can be seen that the reflection coefficient and the transmission coefficient of the device with incident wave height of H=0.06m are mostly larger than those of the wave height of H=0.03m, and the dissipation coefficient of the system decreases with the increasing wave height, which illustrates that the combined OWC-OB system performs good wave energy absorption for larger incident waves. However, for the case of h=0.4m, the reflection and transmission coefficients of the system are larger at the condition of H=0.03m, this is mainly because when the water depth increase to 0.4m, the opening inlet immersed at the relatively deeper position, which cause the smaller incident waves(H=0.03m) reflected and transmitted on the upper outer surface of the cylindrical device, thus increase the reflection and the transmission modes. Furthermore, there are some local peaks which mainly caused by the resonant motions of the oscillating water in the air chamber. For water depth of h=0.3m, the resonant mode occurs at the range of the incident wave period of 0.9s to 1.0s and 1.0s to 1.1s, respectively.

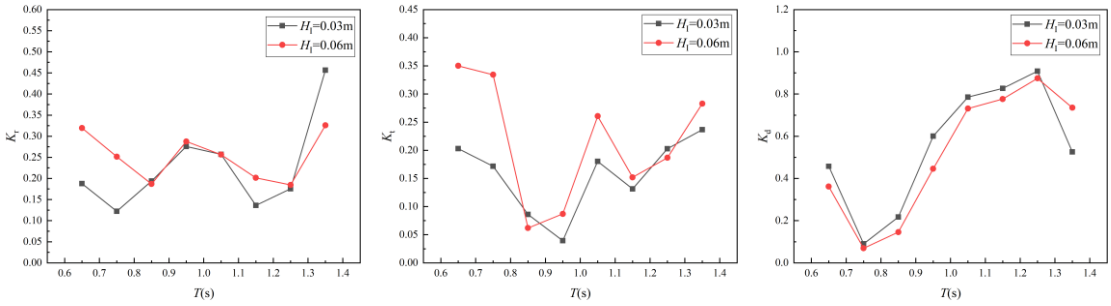

(a) reflection coefficient (b) transmission coefficient (c) dissipation coefficient

Fig.7 Values of K_r, K_t, and K_d with different incident wave heights at h=0.3m

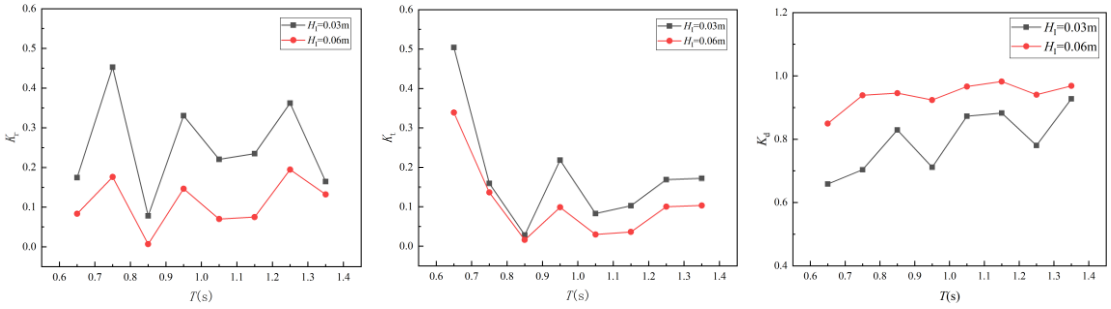

(a) reflection coefficient (b) transmission coefficient (c) dissipation coefficient

Fig.8 Values of K_r, K_t, and K_d with different incident wave heights at h=0.4m

4.2 Influence of Wave Parameters on Hydrodynamic Performance of OWC

In order to highlight the effects on the first energy conversion of the OWC performance, the detailed dynamic characteristics of the OWC device is further studied with the relative wave period T ranges from 0.6s to 1.4s. A series of monitoring points were set around the floater and in the inner chamber of the OWC on the water free surface. Fig.9 displays the distribution location of each monitoring point, where points A-D were located and set in the inner chamber of the fixed OWC device, and points E-G were located near the floater surface. The variation of the hydrodynamic behavior of the OWC device is plotted versus the wave period with H=0.03m and H=0.06m in Fig.13. The water motions, the wave velocity, the air pressure, and the volume flux characteristics are discussed in this subsection.

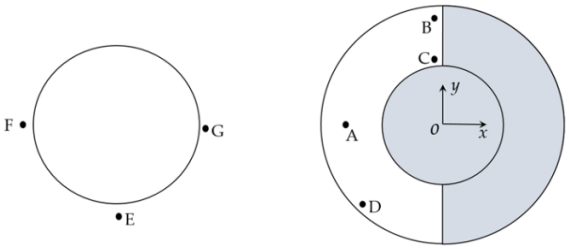

Fig.9 Sketch of the layout of combined floater and semi-arc air chamber with monitoring points A–G.

Fig.10 (a)-(b) depicts the variation of the maxima and minima of the water motions in the chamber, it shows that the wave motions at points A-D in the chamber has an increasing trend within the wave periods from 0.6s to 1.0s and then tends to decrease with the increasing wave period, getting the local peaks at T=0.95s. It is also found that the oscillating motions in the chamber have the larger amplitude at the inner corner area of the chamber (points B and D), whilst the water motions near the opening inlet area (points A and C) performed relatively lower oscillating modes. The hydrodynamic parameters including the water surface elevation, the wave velocity, the air pressure, the volume flux and the wave force at condition of H=0.06m are larger than those of H=0.03m. For the wave velocity at the four points A-D, as is seen in Fig.10(c)-(d), when the incident wave period smaller than the resonant corresponding period(T=0.95s), the velocity at the measured points increased with the increasing wave period. This is related to the fact that the larger water motions oscillated in the air chamber leads to greater wave velocity effects and larger pressure. When the incident wave period larger than 0.95s, the wave velocity decrease with the increasing wave periods. It can be observed that the wave height effect on the oscillation velocity at point D is larger than that at points A, especially for shorter waves, which illustrates that the variation of the wave velocity at the opening inlet area is relatively small.

Figs.10(e)-(h) show the dynamic performance of the air in both the chamber and the nozzle area, including the air pressure, the air volume flux, and the air flow velocity. With respect to the wave motion, the air pressure, volume flux and air flow velocity have the similar trend against different wave periods and wave heights. Compared with the air pressure at the nozzle area on the top of the OWC device, the maximum amplitude of the air pressure in the chamber performed nearly four times larger than that in the nozzle area at the resonant corresponding period of T=0.95s, for both H=0.06m and H=0.03m. The measured point was set at the center position of the nozzle cross section, for the minimum value of the air pressure amplitude with wave height of H=0.06m, the air pressure decreased first until reach the peak point, and then increased to meet its second peak value at T=1.15s, following an increasing trend with wave period enlarged. The air volume flux and the air velocity at the nozzle are presented in Fig.10(g) and Fig.10(h), respectively. With the wave period increased, the maximum amplitude of the volume flux and the air velocity increased from T=1.25s to T=1.35s at the wave height of H=0.03m, which can be also observed in the velocity and motion modes for this same condition. The wave force on the OWC surface was additionally investigated, as is seen in Fig.10(i), the peak and valley points occurred at T=0.95s and T=1.25s, respectively. When the wave period is larger than T=1.25s, the wave force acting on the outer surface of the OWC increased obviously, even for other characteristics were still in decreasing trend, which illustrates that the hydrodynamic performance of the OWC (water motions, the wave velocity, the air pressure and the volume flux characteristics) caused by the resonant mode are not only depends on the incident wave period, will also be affected by the larger wave height.

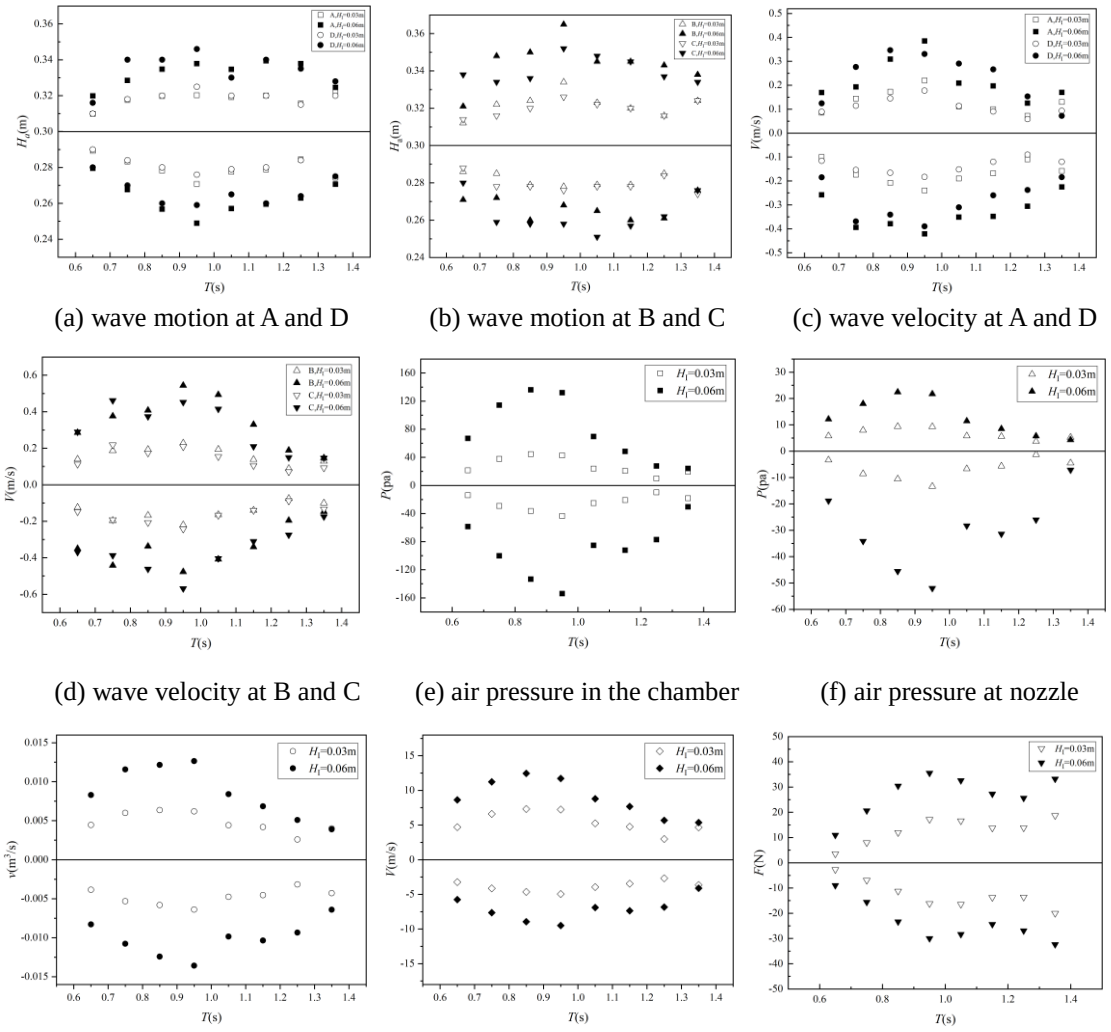

(a) wave motion at A and D (b) wave motion at B and C (c) wave velocity at A and D

(d) wave velocity at B and C (e) air pressure in the chamber (f) air pressure at nozzle

(g) volume flux at nozzle (h) air velocity at nozzle (i) wave force on OWC

Fig.10 Dynamic performance in the OWC chamber and nozzle area with different wave periods

5 Power conversion efficiency

5.1 Mathematical model

The continuity and momentum equations of the incompressible flow are defined as in Eq. (11) and Eq. (12) as follow:

$$\frac{\partial u_i}{\partial x_i} = 0 \tag{11}$$

$$\rho \frac{Du_i}{Dt} = -\frac{\partial P}{\partial x_i} + \left(\mu + \mu_t\right) \frac{\partial}{\partial x_j} \left(\frac{\partial u_i}{\partial x_j} + \frac{\partial u_j}{\partial x_i} \right) + f_i \tag{12}$$

where u_i, t, P, f_i, ρ, μ and μ_t are the velocity components, time, static pressure, body forces, water density, dynamic viscosity, and turbulence viscosity. In the research, μ_t was calculated using the standard k-ω turbulence model. Due to the numerical multi-phase flow model, a large difference between the density of air and water can lead to an overproduction of turbulence at the free surface [36]. In Star-CCM+ software this unreal overproduction of turbulence at the free surface can be reduced by introducing a turbulence damping term which is available in k-ω based models.

The Eulerian multi-phase flow model employs incompressible Reynolds-Averaged Navier-Stokes

equations (RANS) for a water-air mixture. The saturation of the water in a particular volume is denoted by V_i. for V_1=0 and V_2=1, it represents the air above the water-air surface, and for V_1=1 and V_2=0 it represents the water below the water-air surface. The air-water interface is treated as a thin layer of the water-air mixture and have the condition of $0<V_1$, $V_2<1$ & $V_1+V_2=1$.

The volume fraction of each cell which is located at the free surface can be computed using Eq. (13):

$$\frac{\partial V_i}{\partial t}+u_j\frac{\partial V_i}{\partial x_j}=0 \tag{13}$$

where *i* indicates the phase.

Values of μ and ρ can be calculated easily at each cell using a simple volume average over the cell:

$$\rho=V_1\rho_1+V_2\rho_2 \tag{14}$$

$$\mu=V_1\mu_1+V_2\mu_2 \tag{15}$$

The flux of the incidence wave power can be expressed as:

$$P_{\text{in}}=\frac{1}{8T}\rho g H_{\text{I}}^2 DL\cdot n \tag{16}$$

where g, H_I, D, L, n and T are the gravitational attraction, wave height of incidence wave, diameter of the cylinder, water length, the flux coefficient and wave period, respectively. And the flux coefficient n can be calculated by Eq. (17):

$$n=\frac{1}{2}\left[1+\frac{2kd}{\sinh 2kd}\right] \tag{17}$$

where k and d represent the wave number and water depth, respectively.

Also, the output power is averaged over a period and given by:

$$P_{\text{out-OB}}=\frac{b_{\text{PTO}}}{nT}\int_0^{nT}V(t)^2dt \tag{18}$$

$$P_{\text{out-OWC}}=\frac{1}{nT}\int_0^{nT}P(t)q(t)dt \tag{19}$$

where V(t) is the velocity of the buoy, P(t) and q(t) are the air pressure in the chamber and the air volume flow rate across the PTO nozzle area, allowing the variation with time t. Involving the incident wave power P_{in} and output power P_{out}, the conversion efficiency of the OB-OWC device can be calculated as:

$$\eta=\frac{P_{\text{out-OB}}+P_{\text{out-OWC}}}{P_{\text{in}}} \tag{20}$$

5.2 Comparison with single OB and OWC

To investigate the interactions between the OWC and OB, three different models were considered, they are: I) a single OWC; II) a single OB; III) combined OWC-OB system. The presence of the OWC device acting as a breakwater may affect the OB performance in the combined system due to the wave reflection and diffraction from the OWC structure. The water depth was set as h=0.3m, two cases with the normalized incident wave height of 0.03m and 0.06m were considered for modelling. The distance between the OWC and OB device was D/h=4, and the volume ratio of the air chamber and the floater was V_1/V_2=4.6.

Fig.11 shows the comparison analysis of the wave energy conversion efficiency of the hybrid system among the three different models: I), II) and III). In the Figure, with the increasing of the incident wave period, the conversion efficiency of the hybrid device increased to its resonant peak and then decreased.

For different wave conditions and different model (I, II, and III), the corresponding resonant periods relative to the largest conversion efficiency are different. Compared to Fig.11 (c-d), the variation trend of the conversion efficiency of the floater OB against wave period in cases II and III are similar for different wave heights. From the results it can be clearly observed that after combing the floater OB to the OWC device, the wave energy extraction efficiency of OB increased obviously comparing with the single OB in model II, except in the period range from 0.95s to 1.05s. This is mainly because of the reflection of the incident waves acting on the fixed OWC device, which directly caused the reduce of the conversion efficiency of the OWC in the combined system (model III) with wave period ranged from 0.65s to 0.75s for wave height of H=0.03m (see Fig.11(c)). That is to say, the position of the opening inlet set in the front wall of the OWC device will importantly affect the wave energy conversion efficiency for both the floater OB and the fixed OWC device, with conditions of different incident wave height. Thus, the geometrical optimization of the opening inlet of the OWC should be thoroughly discussed in further study.

Fig.11(c) and (d) show the comparison of the wave energy conversion efficiency of the OWC device involved in the model I and model III. When the wave height getting increased, the conversion efficiency of the OWC device increased for both the single OWC and the OWC in combined system. Comparing with the single OWC device, except of conditions for T= 0.65s -0.75s which has been discussed above, it can be seen from the results of the conversion efficiency that the OWC in combined system has better absorption performance obviously at shorter waves, whilst for longer waves, the single OWC device performs well wave extraction ability.

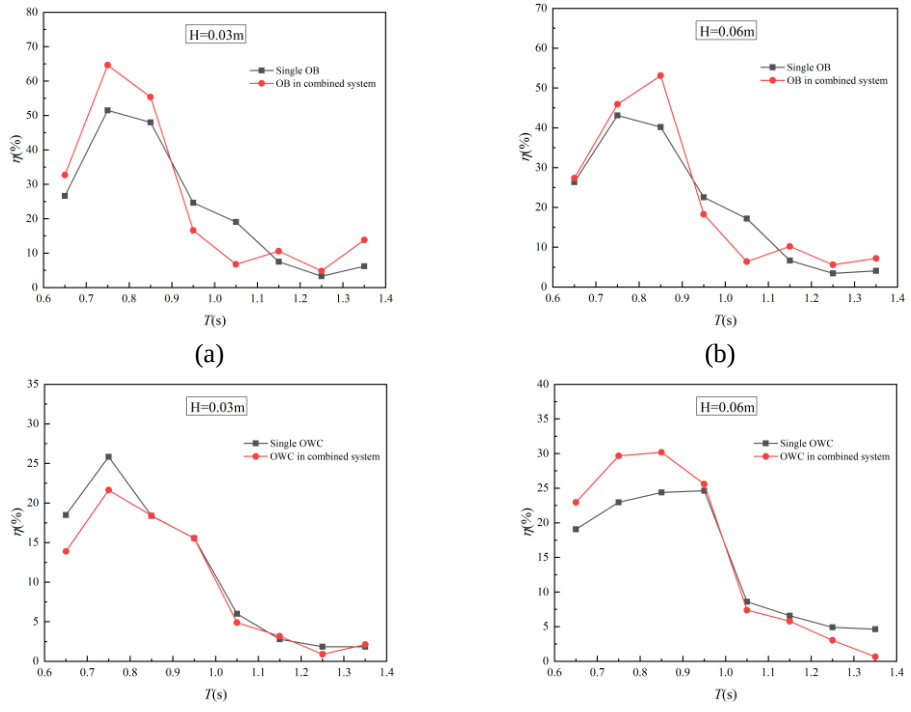

Fig.11 Comparison of η between single OB, single OWC and OB-OWC hybrid system for different wave heights.

5.3 Influence of geometric parameters on conversion efficiency

In this subsection, the influence of geometric parameters of the integrated OB-OWC device on wave energy extraction performance is studied. The effect of opening height on conversion efficiency η is firstly investigated. Fig.12 shows the variation of the conversion efficiency of: i) the combined OB-OWC

system (Fig.12a); ii) the OWC in combined system (Fig.12b); iii) the OB in combined system (Fig.12c) with wave condition of H=0.3m and h=0.06m.

As shown in Fig.12(a), three different conditions of opening height of h_1/h_2=0.3, 0.4 and 0.6 are considered, where h_1 is the submergence of the floater OB, and h_2 is the height of the opening inlet on the OWC front wall. It can be seen that the main peak of the conversion efficiency of the OB-OWC device occurs at the range of 0.75s<T<0.85s, while the other peak occurs at the incident wave period of T=1.15s. The conversion efficiency with different opening height ratio increased first and then decreased with the increasing period, reaching a minimum of η=9.5% at T=1.05 s, and then the conversion efficiency oscillated below 20% within the range of T=1.1s-1.4s.

For the total conversion efficiency of the combined OB-OWC system, among three cases the maximum conversion efficiency of the system is η=83.28% at the period of T=0.85s with h_1/h_2=0.4, it can be also found that the hybrid system with the opening height ratio of h_1/h_2=0.4 has the largest wave energy conversion efficiency for most modelling regime. The second peak of the conversion efficiency occurs at T=1.15s and can reach the value of 16% for longer wave extraction. And for condition of h_1/h_2=0.3, the main peak value is 69.99% which is larger than that of 68.12% for h_1/h_2=0.6.

Meanwhile, Fig.12(b) and (c) show the conversion efficiency of the individual OWC and OB device in the combined hybrid system. The effect of the opening height ratio is sensitive on the OWC conversion efficiency, as seen in Fig.12(b), the relative difference of the conversion efficiency η between two cases of h_1/h_2=0.4 and h_1/h_2=0.3 at the corresponding resonant period T=0.85s reached to 38%, and it can be observed that the peak corresponding period for the resonant mode variated with different h_1/h_2. As the wave period decreased, the peak corresponding resonant period shift towards to the short period region. In other words, with the floater in front of the OWC device, the peak caused by the resonance mode shifts towards to higher frequency region with the increase of the ratio h_1/h_2. However, with the opening height further increased, the opening inlet is no longer submerged, which caused the air in the chamber escaping through it. Needless to say, the wave climate and tidal range at the site of deployment must be considered in determining the submergence and opening height. Additionally, for floater OB in the combined OWC-OB system, as is seen in Fig.12(c), the opening height ratio has little effect on the OB conversion efficiency, only except for the resonant mode(T=0.75-0.85s) in high frequency zone and range of T=1.15-1.35s in low frequency zone, which is mainly caused by the reflection of the OWC with its baffle wall (involving of different opening inlet height effects) and better wave extraction ability of this proposed integrated system for longer waves, respectively.

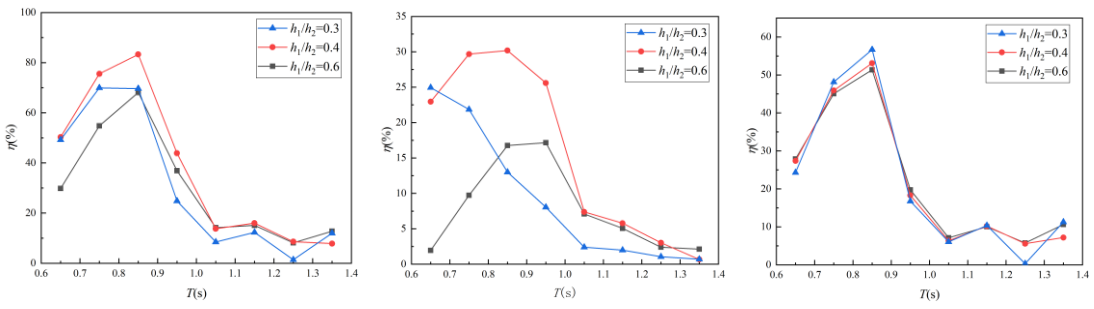

(a) (b) (c)

Fig.12 Comparison of η with T for h_1/h_2=0.3, 0.4 and 0.6 on (a) OB-OWC hybrid system; (b) OWC in combined system; (c) OB in combined system.

Then, the effect of the volume ratio of the air chamber to the floater of the combined OWC-OB

system on the wave power extraction efficiency are additionally studied. Three volume ratios of V_1/V_2=2.3, 3.4 and 4.6 were selected for evaluating the conversion efficiency of the system, where V_1 and V_2 are the volume of OWC chamber and volume of floater OB, respectively. To simplify the complicated influences of the multi-factors of the structures and focus on the volume ratio impacts, the volume of the floater OB was fixed and set as the same parameter with the above model. For the OWC model, the outer diameter of the OWC device is 0.35m and the inner diameter is 0.14m, three angle of the baffle wall was considered to adjust the volume ratio as θ = 90°, 135° and 180° in the air chamber of the OWC. In the following analysis, the opening height ratio of the system was set to h_1/h_2=0.4, the wave height and the water depth were kept the same as H=0.3m and h=0.06m, respectively.

Fig. 13 shows the conversion efficiency of the proposed system with different volume ratios of the OWC-OB device. As seen in Fig.13(a) and (b), it can be found that the largest wave energy conversion efficiency occurs at the condition of V_1/V_2=4.6, for both the efficiency of the OWC-OB and the OWC efficiency in the combing system with the maximum efficiency of 83.28% and 30.18%, respectively. In Fig.13(b), the larger volume ratio of the system (with V_1/V_2 =4.6) can greatly improve the hydrodynamic efficiencies of the system in high frequency zone(T=0.65s-0.95s), and weakening the bimodal effect in resonant mode which could be observed in the condition of V_1/V_2=2.3 and 3.4, to avoid the decrease trend and make it working in a stable state with highly conversion efficiency. By comparing the main peak and the frequency bandwidth of the wave energy capture among these three cases, it can be seen that the peak value and the frequency bandwidth increased with the increasing volume ratio, which could be concluded that the larger volume of the OWC chamber could increase the frequency bandwidth and the hydrodynamic efficiency of the OWC device as well as the total conversion performance for this proposed hybrid OWC-OB system. Besides, the conversion efficiency of the floater OB in the combined system was further evaluated and shown in Fig.13(c). On the contrary, the effect of the volume ratio V_1/V_2 on the conversion efficiency of OB is not apparent and the conversion efficiency decreased with the increasing volume ratio for most incident periods. This is because the enlarged OWC volume absorbed more energy from the incident waves and reduced the wave reflection acting on the floater OB, which resulting in the lower wave energy conversion efficiency and the relative narrow frequency bandwidth compared with other two cases.

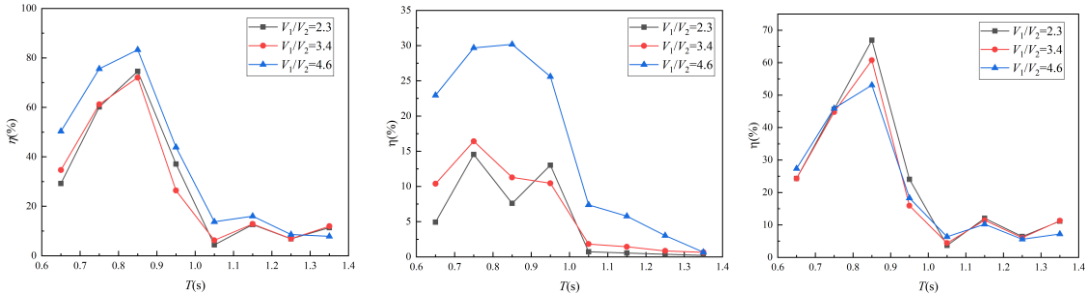

(a) (b) (c)

Fig.13 Comparison of η with T for V_1/V_2=2.3, 3.4 and 4.6 on (a) OB-OWC hybrid system; (b) OWC in combined system; (c) OB in combined system.

6.Conclusion

In this paper, hydrodynamic performance of a combined OWC-OB hybrid WEC system integrating into a fixed breakwater was investigated numerically. The effects of the PTO damping and the geometrical dimensions of both the floater OB and the OWC device on the performance of the system was emphasized. The comparison between each model and the combined system on the efficiency of the

device was analyzed. The following conclusions can be drawn:

1) The wave energy conversion efficiency can approach 83.28% when a heaving floater located in front of the wave chamber. Correspondingly, the resonant wave period occurs at the range of T=0.75s-0.95s. Both the excellent wave power extraction performance and the wave attenuation can be obtained simultaneously for this proposed system.

2) Under the test conditions, the height of the opening inlet has significant effects on the conversion efficiency of the proposed combined system. The hybrid system with the opening height ratio of h_1/h_2=0.4 has the largest wave energy conversion efficiency for most modelling regime, and the peak corresponding period shifts towards to high frequency region with the increase of the ratio h_1/h_2.

3) Comparing with the conversion efficiency of the OB in the combined system, the main peak and the frequency bandwidth of the wave energy capture increased with the increasing volume ratio V_1/V_2, the larger volume ratio for V_1/V_2 =4.6 can greatly improve the hydrodynamic efficiencies of the system in high frequency zone and weakening the bimodal effect in resonant mode, whilst the opposite trend observed in the OB model when the volume ratio increased.

The results of the numerical study allow to predict the hydrodynamic characteristics and the wave energy conversion performance of the proposed hybrid system. The combined OWC-OB system can be applied at the offshore site to meet both the breakwater function and the wave energy utilization requirement. Due to the wave reflection acting on the OB device, the hydrodynamic efficiency of the floater would be directly affected by the geometrical dimension of the opening inlet of the OWC device, and considering of the wave resonance, the wave focusing effect is beneficial for the wave energy conversion efficiency improvement. Hence, further studies are needed to focus on the concentrated wave effects for the hybrid WEC array by arranging the cylindrical devices in concave arcs, and the comprehensive optimization of the geometrical dimensions of the combined OWC-OB system.

Acknowledgement

This paper is financially supported by the National Natural Science Foundation (Grant No.52101306 and No.52071095 and No. 51979063), the National Science Foundation of Shandong Province (Grant No. ZR2021QE121), National Science Foundation of Heilongjiang Province (Grant No. LH2021E049), the Open Foundation of State Key Laboratory of Coastal and Offshore Engineering of Dalian University of Technology [LP2006], the British Council (BRI JOINT project) and EPSRC ResIn project (EP/R007519/1) who part funded the corresponding author, and the China Scholarship Council (award to Yang Can for study abroad at the University of Exeter). Special thanks go to TORC and the anonymous reviewers for their careful reading of the manuscript and valuable comments.

Reference

[1] United Nations Environment Programme. Global trends in sustainable energy investment, analysis of trends and issues in the financing of renewable energy and energy efficiency in OECD and developing countries. 2007.

[2] Edenhofer O, Madruga RP, Sokona Y, Seyboth K, Matschoss P, Kadner S, et al. Renewable energy sources and climate change mitigation: special report of the intergovernmental panel on climate change. Cambridge University Press; 2012.

[3] K. Rezanejad, J. Bhattacharjee, C. Guedes Soares. Analytical and numerical study of dual-chamber oscillating water columns on stepped bottom. Renewable Energy 2015; 75: 272-282.

[4] Galarraga I, Eguino MG, Markandya A. Handbook of sustainable energy. Edward Elgar Publishing, Inc; 2011.
[5] Emre Ozkop, Ismail H. Altas. Control, power and electrical components in wave energy conversion systems: A review of the technologies. Renewable and Sustainable Energy Reviews 2017; 67: 106–115.
[6] S. Astariz, G. Iglesias. The economics of wave energy: A review. Renewable and Sustainable Energy Reviews 2015; 45: 397-408.
[7] Graw, K.U. Wave energy breakwaters-a device comparison. In Proceedings of the Conference in Ocean Engineering, Madras, India, 17–20 December 1996.
[8] Yijin Liu, Ye Li, Fenglan He, Haifeng Wang. Comparison study of tidal stream and wave energy technology development between China and some Western Countries. Renewable and Sustainable Energy Reviews 2017; 76: 701–716.
[9] Suzuki, M., Arakawa, C., Takahashi, S. Performance of wave power generating system installed in breakwater at Sakata port in Japan. In Proceedings of the Fourteenth International Offshore and Polar Engineering Conference, Toulon, France, 23–28 May 2004.
[10] Falcão, A.F.O. The shoreline OWC wave power plant at the Azores. In Proceedings of the 4th European Wave Energy Conference, Aalborg, Denmark, 4–6 December 2000.
[11] Henriques, J., Portillo, J., Sheng, W., Gato, L., Falcão, A. Dynamics and control of air turbines in oscillating-water-column wave energy converters: Analyses and case study. Renewable and Sustainable Energy Reviews 2019; 112: 571–589.
[12] Healt, T., Whittaker, T., Boake, C. The design, construction and operation of the LIMPET wave energy converter (Islay, Scotland). In Proceedings of the 4th European Wave Energy Conference, Aalborg, Denmark, 4–6 December 2000.
[13] Dahai Zhang, Wei Li, Yonggang Lin. Wave energy in China: current status and perpesctives. Renewable Energy 2009; 34: 2089-2092.
[14] Siming Zheng, Yongliang Zhang, Gregorio Iglesias. Coast/breakwater-integrated OWC: A theoretical model. Marine Structures 2019; 66: 121-135.
[15] Shi, H., Yang, G., Liu, Z. Study on New Caisson Breakwater as OWC. Periodical of Ocean University of China (Natural Science Edition), China 2010; 40: 142-146.
[16] Rafael A.A.C. Gonçalves, Paulo R.F. Teixeira, Eric Didier, Fernando R. Torres. Numerical analysis of the influence of air compressibility effects on an oscillating water column wave energy converter chamber. Renewable Energy 2020; 153: 1183-1193.
[17] Medina Rodríguez AA, Blanco Ilzarbe JM, Silva Casarín R, Izquierdo Ereño U. The Influence of the Chamber Configuration on the Hydrodynamic Efficiency of Oscillating Water Column Devices. Journal of Marine Science and Engineering. 2020; 8(10):751.
[18] Dezhi Ning, Rongquan Wang, Lifen Chen, Ke Sun. Experimental investigation of a land-based dual-chamber OWC wave energy converter. Renewable and Sustainable Energy Reviews 2019; 105: 48-60.
[19] Rongquan Wang, Dezhi Ning, Qingping Zou. Wave loads on a land-based dual-chamber Oscillating Water Column wave energy device. Coastal Engineering 2020; 160: 103744.
[20] K. Rezanejad, J. Bhattacharjee, C. Guedes Soares. Analytical and numerical study of dual-chamber oscillating water columns on stepped bottom. Renewable Energy 2015; 75: 272-282.
[21] Ali Taherian Haghighi, Amir H. Nikseresht, Mohammad Hayati. Numerical analysis of hydrodynamic performance of a dual-chamber Oscillating Water Column. Energy 2021; 221: 119892.

[22] Tanimoto, K.; Takahashi, S.; Kimura, K. Structures and hydraulic characteristics of breakwaters the state of the art of breakwater design in Japan. Report of Port and Harbour Research Institute. 1987; 26: 11-55.

[23] Chen, J., Wang, Y., Wang, G., Cai, L. Wave energy conversion efficiency of the dual cylindrical caisson breakwaters embodying an OWC with a semi-arc inlet on outer wall. In: ASME 2017 36th International Conference on Ocean, Offshore and Arctic Engineering (OMAE2017). Norway: Trondheim; 2017.

[24] Jing Chen, Hongjie Wen, Yongxue Wang, Bing Ren. Experimental investigation of an annular sector OWC device incorporated into a dual cylindrical caisson breakwater. Energy 2020; 211: 118681.

[25] X.L. Zhao, D.Z. Ning, C.W. Zhang, Y.Y. Liu, H.G. Kang. Analytical study on an oscillating buoy wave energy converter integrated into a fixed box-type breakwater. Mathematical Problems in Engineering 2017; 2017: p9

[26] X. Zhao, D. Ning. Experimental investigation of breakwater-type WEC composed of both stationary and floating pontoons. Energy 2018; 155: 226-233.

[27] Hengming Zhang, Binzhen Zhou, Christopher Vogel, Richard Willden, Jun Zang, Jing Geng. Hydrodynamic performance of a dual-floater hybrid system combining a floating breakwater and an oscillating-buoy type wave energy converter. Applied Energy 2020; 259: 114212.

[28] Zheng S, Zhang Y. Analytical study on wave power extraction from a hybrid wave energy converter. Ocean Engineering 2018; 165: 252-263.

[29] Zheng S, Zhang Y. Theoretical modelling of a new hybrid wave energy converter in regular waves. Renewable Energy 2018; 128A: 125-141.

[30] Lin Cui, Siming Zheng, Yongliang Zhang, Jon Miles, Gregorio Iglesias. Wave power extraction from a hybrid oscillating water column-oscillating buoy wave energy converter. Renewable and Sustainable Energy Reviews 2021; 135: 110234.

[31] Falcão AF, Henriques JC. Oscillating-water-column wave energy converters and air turbines: a review. Renewable Energy 2016; 85: 1391-424.

[32] López I, Castro A, Iglesias G. Hydrodynamic performance of an oscillating water column wave energy converter by means of particle imaging velocimetry. Energy 2015; 83: 89-103.

[33] Sun SY, Sun SL, Wu GX. Fully nonlinear time domain analysis for Hydrodynamic performance of an oscillating wave surge converter. China Ocean Engineering 2018; 32(5): 582–92.

[34] Zhou BZ, Ning DZ, Teng B, Bai W. Numerical investigation of wave radiation by a vertical cylinder using a fully nonlinear HOBEM. Ocean Engineering 2013; 70: 1-13.

[35] Zhou BZ, Wu L, Xu GD. Resonance of the roll motion of a two dimensional barge induced by triple frequency wave force. Ocean Engineering 2017; 134: 13-23.

[36] Kamath A, Bihs H, Arntsen QA. Numerical investigations of the hydrodynamics of an oscillating water column device. Ocean Engineering 2015; 102:40-50.

Dear Editors:

We would like to submit the enclosed manuscript entitled “Numerical investigation of a dual cylindrical OWC hybrid system incorporated into a fixed caisson breakwater”, which we wish to be considered for publication in “Energy”. No conflict of interest exits in the submission of this manuscript, and manuscript is approved by all authors for publication. I would like to declare on behalf of my co-authors that the work described was original research that has not been published previously, and not under consideration for publication elsewhere, in whole or in part. All the authors listed have approved the manuscript that is enclosed.

In this work, a novel cylindrical oscillating water column (OWC) combining with a heaving oscillating buoy incorporated into a fixed caisson type breakwater was investigated to study the dynamic behaviour and the wave energy conversion efficiency of the proposed OWC device. The modeled results of the hydrodynamic performance of the integrated system compared with the published tank test data and the validations are at model scale. Based on the numerical simulation, the influences of different turbine damping and geometrical configurations of the OWC chamber and OB model on the wave energy conversion efficiency were analyzed to improve the understanding of the flow field performance in the air chamber of the OWC device subjected to waves. I hope this paper is suitable for " Energy”.

We deeply appreciate your consideration of our manuscript, and we look forward to receiving comments from the reviewers. If you have any queries, please don’t hesitate to contact me at the address below.

Thank you and best regards.

Yours sincerely,
Can Yang
College of Shipbuilding Engineering,
Harbin Engineering University, China;
College of Engineering, Mathematics and Physical Sciences,
University of Exeter, UK
E-mail: c.yangdlut@163.com
L.Johanning@exeter.ac.uk

Declaration of interest statement

The authors declare that they have no known competing financial interests or personal relationships that could have appeared to influence the work reported in this paper.

All authors